Deformation and failure of curved colloidal crystal shells

Carlotta Negri[a,b], Alessandro L. Sellerio[a], Stefano Zapperi[a,b,c,d], and M. Carmen Miguel[e,1]

[a]Center for Complexity and Biosystems, Department of Physics, University of Milan, 20133 Milan, Italy; [b]Institute for Scientific Interchange Foundation, 10126 Turin, Italy; [c]Istituto per l'Energetica e le Interfasi, Consiglio Nazionale delle Ricerche, 20125 Milan, Italy; [d]Department of Applied Physics, Aalto University, 11100 FI-00076 Aalto, Finland; and [e]Departament de Física Fonamental, Facultat de Física, Universitat de Barcelona, 08028 Barcelona, Spain

Edited by David A. Weitz, Harvard University, Cambridge, MA, and approved October 13, 2015 (received for review September 17, 2015)

Designing and controlling particle self-assembly into robust and reliable high-performance smart materials often involves crystalline ordering in curved spaces. Examples include carbon allotropes like graphene, synthetic materials such as colloidosomes, or biological systems like lipid membranes, solid domains on vesicles, or viral capsids. Despite the relevance of these structures, the irreversible deformation and failure of curved crystals is still mostly unexplored. Here, we report simulation results of the mechanical deformation of colloidal crystalline shells that illustrate the subtle role played by geometrically necessary topological defects in controlling plastic yielding and failure. We observe plastic deformation attributable to the migration and reorientation of grain boundary scars, a collective process assisted by the intermittent proliferation of disclination pairs or abrupt structural failure induced by crack nucleating at defects. Our results provide general guiding principles to optimize the structural and mechanical stability of curved colloidal crystals.

topological defects | curved crystals | fracture | plastic deformation | plastic avalanches

The morphology of crystals becomes peculiar when self-assembled on curved shells. For example, the Gaussian curvature of a sphere demands the presence of geometrically necessary rotational defects (disclinations) such as the 12 pentagons in a soccer ball. Disclinations can be found in thin shell structures at different length scales: from the world of carbon allotropes (1) [as in fullerenes, nanotubes, and graphene (2)] to biological systems [such as in lipid membranes (3), solid domains on vesicles (4, 5), or in viral capsids (6–8)], and in synthetic structures such as colloidosomes, colloidal particle shells lying at the interface between two fluids (9–12). Thin-shell structures are often conceived for encapsulation purposes at various scales (i.e., as delivery vehicles of different kinds of cargo, from drugs to flavors and cosmetics) and arise naturally in biological systems. Examples include crystalline and glassy colloidosomes, capsules of Janus and patchy particles, nematic vesicles, and viral capsids.

Theoretical considerations indicate that arranging a colloidal crystal into a curved geometry involves elastic deformation and the presence of geometrically necessary disclinations showed by simulations to be attached to extended grain boundary scars (13–15), as also confirmed in several experiments (5, 9, 16, 17). Thus, grain boundary scars are different from standard grain boundaries in that they have a nonzero disclination charge, which makes them more costly. Such a complex topological structure is bound to interfere with the mechanical response of the shell in a way that is still unclear. Understanding this point, however, is of utmost importance to control the deformation of many functionalized self-assembled materials (9, 18, 19). Numerical and theoretical approaches to date are typically based on solving the elasticity field between grain-boundary scars and deriving equilibrium particle configurations from the effective free energy of the interacting defects (15, 20–23). Dynamic models have also been considered (24) to describe the experimentally observed dislocation gliding within the grain-boundary scars (5), or to precisely relate the crystallization dynamics to the surface curvature (25), but no studies so far have inspected the stress–strain relationships or the microstructural reorganizations occurring in response to different protocols of deformation of curved crystals under load.

Here, we study the mechanical response of crystalline colloidal shells by molecular dynamics simulations. To this end, we consider a crystal made by colloidal particles confined to the surface of a sphere and then analyze its response to geometrical changes of this surface. We first simulate an isotropic inflation of the sphere, which induces tensile stresses in the crystal, leading eventually to its failure. Geometrically necessary scars act in this case as weak spots where fracture is nucleated. Next, we consider shape deformations that modify the local curvature, such as the squeezing of the sphere. In particular, we discuss shape deformations that preserve the shell surface area, so that stretching is not relevant. In this case, the crystal deforms irreversibly and intermittently by reorganizing and reorienting its grain boundary scar structure. Nevertheless, disclinations and/or scars do not seem to glide easily through the crystal. We observe that these defects only move through the reaction with new dislocations that are nucleated in the crystal along the deformation process. To better understand the motion of disclinations and scars, we also study the response of the crystal to a localized deformation attributable to indentation that leads to the formation of a hole in the crystal. The newly created hole changes the crystal topological characteristics and provokes the reorganization of its existing scar structure. We corroborate that the basic microscopic mechanism undergoing scar motion always requires the assistance of new dislocations. All of these peculiar microscopic processes trigger a heterogeneous response in the form of scale-free plastic avalanches (26, 27). The scaling properties of plastic deformation in curved geometries, however, are observed to deviate from the statistical behavior experimentally and numerically observed for similar phenomena in flat geometry.

Significance

Substantial experimental and theoretical work has been devoted to understand the equilibrium properties of curved crystals, but these crystals' stability under mechanical forces remains largely unexplored and unknown. Understanding how curved crystals can adapt their shape and resist failure is of fundamental importance because these structures are at the forefront in the drive to fabricate new functionalized self-assembled materials. Here, we address these questions by numerical simulations of the deformation of colloidal crystalline shells. Our results highlight the fundamental role played by geometrically necessary crystal defects in controlling mechanical stability and plastic rearrangements of the shell.

Author contributions: C.N., A.L.S., S.Z., and M.C.M. designed research; C.N., A.L.S., S.Z., and M.C.M. performed research; C.N. and M.C.M. analyzed data; and S.Z. and M.C.M. wrote the paper.

The authors declare no conflict of interest.

This article is a PNAS Direct Submission.

Freely available online through the PNAS open access option.

[1]To whom correspondence should be addressed. Email: carmen.miguel@ub.edu.

This article contains supporting information online at www.pnas.org/lookup/suppl/doi:10.1073/pnas.1518258112/-/DCSupplemental.

Model

We consider a set of N colloidal particles confined to a spherical interface and interacting through a pair-wise Lennard-Jones potential

$$V_{\mathrm{LJ}} = 4\epsilon\left[\left(\frac{\sigma}{r}\right)^{12} - \left(\frac{\sigma}{r}\right)^{6}\right] \quad r < r_c, \qquad [1]$$

where ε is a characteristic energy scale, σ a characteristic length scale, and r_c is the cutoff distance that is set equal to $r_c = 4.5\sigma$. All of the particles are initially confined to a spherical surface of radius R by a constraining force field of the form

$$\mathbf{F} = -K(r-R)\frac{\mathbf{r}}{r}, \qquad [2]$$

where K is the spring constant binding the particles to the spherical surface. The potential we use is appropriate to study fracture, a phenomenon that would not occur with a purely repulsive long-range potential. Nonetheless, such repulsive potentials have been commonly considered to explore minimal energy configurations or other purely geometrical features (e.g., see ref. 20).

The geometrical frustration introduced by a nonzero Gaussian curvature makes the perfect triangular crystalline order, characteristic of unbounded flat surfaces, impossible to fit on general curved surfaces in the absence of rotational topological defects. In particular, any triangulation of the sphere is required to have at least 12 fivefold disclinations (i.e., particles with five nearest neighbors instead of six). We choose the interparticle equilibrium distance so as to ideally tessellate the surface of the sphere $S = 4\pi R^2$ with $N-12$ hexagons and 12 pentagons:

$$\sigma = 2^{-1/6}\sqrt{\frac{8\pi R^2}{\sqrt{3}(N-2)}}. \qquad [3]$$

This formula corresponds to an Euclidean lattice spacing equal to the minimum of the pair potential $r_{\min} = 2^{1/6}\sigma$ (i.e., a potential energy landscape given by N minima placed in an hexagonal lattice) and is thus only exact for a tessellation of a flat surface. In our system, small corrections are attributable to curvature but also to height fluctuations or "buckling," which is allowed by the finite stiffness K of the constraining force along the radial direction. To minimize those effects, we choose $R/\sigma \gg 1$ and also $K/K_\sigma \gg 1$, where $K_\sigma \propto \epsilon/\sigma^2$ is the spring constant of the Lennard-Jones potential (Eq. **1**) in the harmonic approximation.

We consider two main deformation modes inducing either volumetric or deviatoric strain in the shell by modifying the constraining force field in Eq. **2**. Volumetric strain is increased by inflating the shell through an isotropic force field:

$$\mathbf{F} = -K(r-R(t))\frac{\mathbf{r}}{r}, \qquad [4]$$

where the radius $R(t)$ grows in time according to $R(t) = R_0 + tv_{\mathrm{exp}}$, and v_{exp} is the expansion velocity.

Deviatoric strain can be induced by changing the shape of the spherical shell into a prolate spheroid, centered at the origin and with principal semiaxes $R\times a(t)$ and $R\times c(t)$, keeping either its volume or its surface constant. This can be achieved by a force field

$$\mathbf{F} = -K(d(t)-R)\frac{\mathbf{r}}{d(t)}, \qquad [5]$$

where $d = \sqrt{(x^2+y^2)/a^2 + z^2/c^2}$, $c(t)$ grows in time with a deformation velocity v_{def}[i.e., $c(t) = 1 + t\,v_{\mathrm{def}}$], and $a(t)$ varies, so that the surface or the volume of the spheroid are conserved. Here, we discuss in detail the case where we preserve the surface area of the crystal.

Molecular dynamics simulations using the prescriptions discussed above are performed with LAMMPS (Large-scale Atomic/Molecular Massively Parallel Simulator: a free, open source Molecular Dynamics Simulator) (28). We use a microcanonical ensemble integration scheme (NVE), but we add a viscous damping force proportional to the velocity of the colloidal particles to drain the kinetic energy from the system in a controlled fashion. Thus, the total energy is not conserved, and the motion is almost overdamped, which is appropriate for best studying colloidal systems. We use convenient dimensionless units throughout the paper, scaling lengths by σ, times by $t_0 \equiv \sqrt{m/K}$, energies by $\epsilon_0 \equiv K\sigma^2$, stresses by $\Sigma_0 \equiv K/\sigma$, and velocities by $v_0 \equiv \sigma\sqrt{K/m}$, where K is the spring constant in Eq. **2**, σ is the Lennard-Jones parameter in Eq. **1**, and m is the mass of the colloidal particles.

Results

Topological Properties of Crystalline Shells. To study the mechanical response of crystalline colloidal shells by molecular dynamics simulations, we first prepare the initial spherical shell configuration by either of the two following cases: case 1, placing the particles at random on the sphere surface, in a very unstable arrangement, and then letting them evolve and rearrange while slowly draining the energy until they get frozen in a stationary configuration; or case 2, placing the particles in a configuration with icosahedral symmetry where only exactly 12 geometrically necessary fivefold disclinations are present, a more stable arrangement, and then letting the particles also freely evolve.

In case 1, the equilibrium shell features 12 grain-boundary scars (i.e., regularly spaced arrays of alternating fivefold and sevenfold disclinations), exactly as expected for $R/\sigma \gg 1$ (15, 20–24). In the latter (case 2), the number of particles must be suited to fit an icosadeltahedral lattice and is chosen as a Caspar and Klug "magic number" $N = 10(\nu^2+\mu^2+\nu\mu)+2$, with μ and ν nonnegative integers. This procedure allows us to start with low-energy configurations of particles interacting isotropically on the surface of a sphere (6, 7). Although this configuration is more prestressed than the previous one (Fig. S1), where the geometric frustration is released by the formation of the scars, this configuration can nonetheless remain stable during this initial preparation phase depending on the value of the ratio K/K_σ, or already relax in a scarred configuration, with small scars that are clearly centered on the previous location of the fivefold defects (Fig. S1).

Fracture Mechanics of Inflated Shells. When the shell is expanded isotropically, the crystal is subject to an increasing volumetric tensile stress Σ_{m} that can be quantified using the trace of the stress tensor σ_{ij}. In particular, we calculate the sum

$$\Sigma_{\mathrm{m}} = \sigma_{xx} + \sigma_{yy} + \sigma_{zz}, \qquad [6]$$

evaluated locally at each particle position, and then average over all particles in the shell to obtain a strain–stress relationship. As shown in Fig. 1*A*, the crystal responds elastically to small deformations, and the average internal stress Σ_{m} increases linearly. At larger deformation, the stress increases nonlinearly and then suddenly drops when the crystal fractures. When we decrease the strength of the interaction between colloidal particles ε, the shell becomes softer, and consequently failure is more ductile, with smaller stress drops. In the limit of very weak attractive interactions, deformation is smoother and the stress drop at failure is very small. Furthermore, scarred configurations fail at smaller strain values and exhibit lower peak stress intensities than ordered icosadeltahedral structures (Fig. S2).

For randomly prepared samples (case 1), fracture nucleates along grain boundary scars (Fig. 1 *B* and *C* and Movies S1 and S2). This behavior is attributable to the fact that grain boundary scars induce weak spots in the crystal, where cracks are easily nucleated. For ordered samples (case 2), cracks nucleate instead in between isolated disclinations and propagate along the lines connecting nearby defects (Fig. S2). The particular distribution

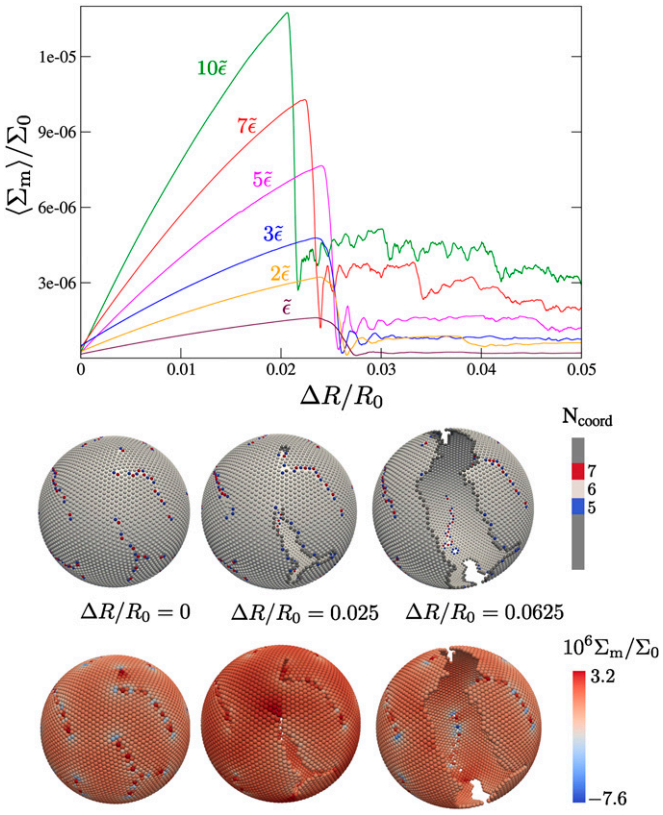

Fig. 1. Curved colloidal crystals under isotropic expansion fracture along defects. (*Upper*) Volumetric stress Σ_m, averaged over all particles, as a function of the relative radius of deformation for different values of the interaction energy ($\tilde{\epsilon} \simeq 7.2\,10^{-6}\,\epsilon_0$). The initial shell configuration (obtained by relaxing a random configuration of particles) shows topological defects already arranged in the form of scars. (*Lower*) Evolution of both the scars configuration and the per-particle volumetric stress at $\epsilon = \tilde{\epsilon}$. We show three different snapshots corresponding to different deformation radii before and after the shell rupture.

of stress fields along these connecting lines favors crack nucleation under these conditions.

We have also repeated our simulations using a number of colloidal particles N that is slightly smaller than the optimal number needed to triangulate the sphere, as dictated by Eq. **3**. Hence, the crystal is initially prestressed, and when it is inflated, it fails at a smaller strain, or it could even break without inflating if prestress is above the breakdown point (see the case $N = 5{,}027$ in Fig. S3). The peak stress, however, does not change significantly (Fig. S3).

Plastically Deformed Shells. To further study the role of curvature in plastic deformation of curved crystals, we now consider the case in which the Lennard-Jones shell changes its shape into a prolate ellipsoid. To be precise, we have chosen to squeeze the spherical shell preserving its surface area, or the mean interparticle distance, to avoid the interference of stretching deformations that would tend to crack the Lennard-Jones shell, as discussed in the previous section. Relevant mechanical information can be extracted in this case from the components of the deviatoric stress tensor, for instance, given the symmetry properties of the prolate ellipsoid, from the zz-component of the deviatoric stress defined as

$$\Sigma_d = \sigma_{zz} - \frac{1}{3}\Sigma_m, \qquad [7]$$

which gives us a measure of nonvolumetric distortions of the body shape. In our analysis, we follow the conventional method of breaking down the stress tensor into two parts: an isotropic part (in Eq. **6**) describing the pressure associated with a volume change and a deviatoric part, describing stresses attributable to shape deformations that do not involve volume changes.

The average stress–strain curve reported in Fig. 2 shows an initial elastic regime followed by intermittent stress drops, a typical feature of plastic deformation in micron-scale crystals (29, 30). In conventional geometries where curvature is not a relevant ingredient, sudden jumps of the stress under strain-controlled deformation tests are known to be attributable to collective irreversible rearrangements of topological defects such as dislocations and grain boundaries. Dislocations glide easily through plastically deforming crystals, leaving several traces of their collective motion, such as sudden stress drops in the stress–strain relations or striking slip bands at the surface of the deformed samples.

In our spherical colloidal crystals, the curvature of a sphere demands the presence of fivefold disclinations or grain-boundary scars, which are different from standard grain boundaries in that they have a nonzero disclination charge. More precisely, the total disclination charge in a spherical crystal should be equal to +12. One can assign a disclination charge q_i to each particle i in the spherical crystal by counting the number of its nearest neighbors c_i and defining the disclination charge as $q_i \equiv 6 - c_i$. In this way, fivefold coordinated particles within a triangular lattice correspond to positive disclinations of topological charge $q = +1$ and sevenfold coordinated particles to negative disclinations with $q = -1$.

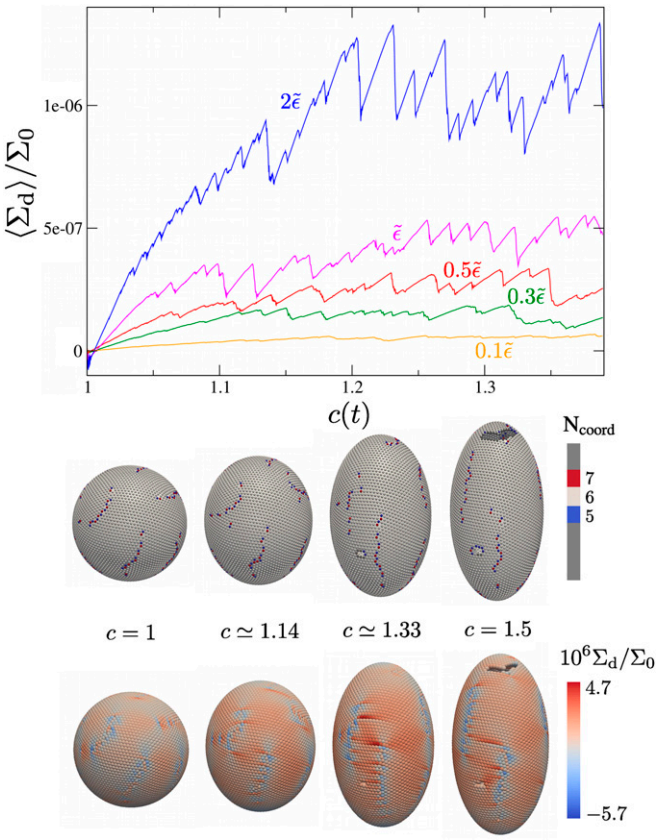

Fig. 2. Squeezing a colloidal crystalline sphere leads to plastic deformation mediated by grain boundary scars reorientation. (*Upper*) Deviatoric stress Σ_d, averaged over all particles, as a function of the ellipsoid semiaxis $c(t)$ for different values of the interaction energy ε ($\tilde{\epsilon} \simeq 1.42\,10^{-6}\,\epsilon_0$). The ellipsoid is deformed at constant surface area. (*Lower*) Evolution of both the scars configuration and the per-particle deviatoric stress at $\epsilon = \tilde{\epsilon}$. We show several snapshots corresponding to different values of the ellipsoid semiaxis $c(t)$ during a deformation test at constant surface and driving velocity $v_{def} = 1.88 v_0\,10^{-7}$.

PHYSICS

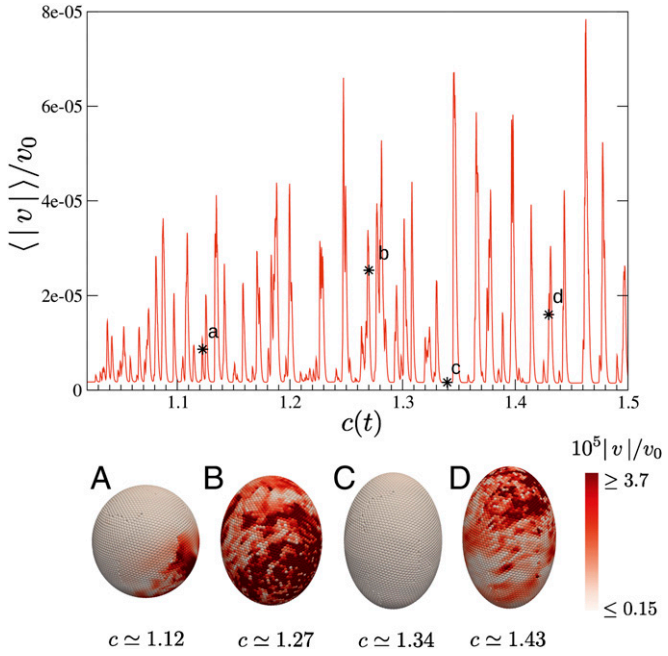

Fig. 3. Plastic deformation is intermittent. (*Upper*) Averaged root mean square velocity for the case $\epsilon = \bar{\epsilon}$ as a function of the spheroid deformation parameter $c(t)$ displays bursts of activity (or avalanches) in correspondence with dislocations rearrangements. (*Lower*) The magnitude of the per-particle velocity, here displayed at several time steps for a deformation test at constant surface and driving velocity $v_{\text{def}} = 1.88\,10^{-7}\,v_0$, helps to visualize the widespread dynamics of avalanches during deformation.

From this point of view, a dislocation is therefore a neutral pair of near-neighbor oppositely charged disclinations, or a fivefold–sevenfold pair. Finally, the disclination charge of a scar will be the sum of individual disclination charges along a defective 5–7–5–⋯ string, and in most of the cases reported here, the charge is equal to +1, because the scars usually contain an unbalanced fivefold particle.

We find that by squeezing the sphere, these twelve +1 grain boundary scars rearrange in a rather intricate manner and eventually reorient along the spheroid axis. This result is also shown in Fig. 2 as well as in Movies S3 and S4. By doing so, the stress fields built up in the crystal loaded under this particular squeezing mode (i.e., under an effective pressure that changes the total volume of the ellipsoid at the expense of preserving its surface area) gets, at least partially, accommodated with the scars reorientation along the axial direction. In the continuum mechanics of thin shells under pressure, the so-called circumferential or hoop stress is known to be about twice as big as the stress in the axial direction (31). This stress is at the base of the lengthwise ripping of a grilled sausage skin, or of the bursting observed in long gas pipes. In our case, the reorientation of the grain boundary scars replaces the rupture of the elastic shell because the reorientation process can also partly accommodate this stress component.

Finally, it is also worth emphasizing that isolated disclinations and/or scars do not glide easily through the crystal in the same way as dislocations normally do to release stress in conventional geometries. Indeed, in our study, we unveil, for instance, that scars only move and reorient through multiple reactions with new dislocations that are nucleated in the strained crystal; that is, scars move by growing longer on one side (i.e., after the attachment of a new, properly oriented dislocation) and getting shorter on the opposite one (i.e., after the annihilation of an existing 5–7 pair with a nearby dislocation of the opposite sign) following this basic microscopic mechanism that requires the assistance of new dislocations. We further inspect and discuss this assisted dynamics performing indentation tests.

Crackling Noise. In Fig. 2, we observe a heterogeneous dynamics in response to the accumulation of internal elastic stress in the crystal. The stress drops in Fig. 2 are also referred to as plastic avalanches (26, 27). Plastic avalanches are widely observed in plastically deforming crystals in response to the nucleation and correlated motion of topological defects. Correlated motion is also at the base of the so-called crackling noise (32), associated to localized avalanches spreading through the crystalline shell. An example of the spatiotemporal intermittency we observe in our simulations is reported in Fig. 3, where we show the averaged root mean square velocity of the colloidal particles and where some of the crackling noise peaks are shown together with the corresponding velocity maps.

To quantify the statistics of crackling noise in curved crystalline shells, we measure the distribution of avalanche sizes, defined as the area under each pulse. This is done in practice by defining a small threshold v_c, and considering as a pulse any sequence of time points where the velocity $\langle |v| \rangle > v_c$. The avalanche size is defined as

$$s \equiv \int_{t_1}^{t_2} dt \langle |v(t)| \rangle, \qquad [8]$$

where t_1 and t_2 are the times where the pulse starts and ends, respectively. The distribution of avalanche sizes are reported in Fig. 4 as a function of the driving rate v_{def}. The threshold v_c has to be larger than the velocity background because of numerical noise but small enough to record the signal. In the present case, a good choice is $v_c = 10 v_{\text{def}}$.

As expected in general for crackling noise, the distribution crucially depends on the deformation rate. For slow deformation, we find that the avalanche distribution decays as a power law, $P(s) \sim s^{-\tau}$, with an exponent close to $\tau = 2$. This value is different from the one measured in flat geometry through 2D dislocation dynamics (33) and colloidal crystal simulations (34), which yield $\tau \simeq 1$. This finding suggests that the shell curvature introduces peculiar properties to the dynamics of plastic avalanches. Indeed, isolated disclinations and/or scars do not seem to move unless assisted by new dislocations, and dislocations themselves do not seem to glide over long distances after nucleating and unbinding on the surface of a spherical shell, because they mainly react with existing scars. Thus, in curved geometries, most of the plastic

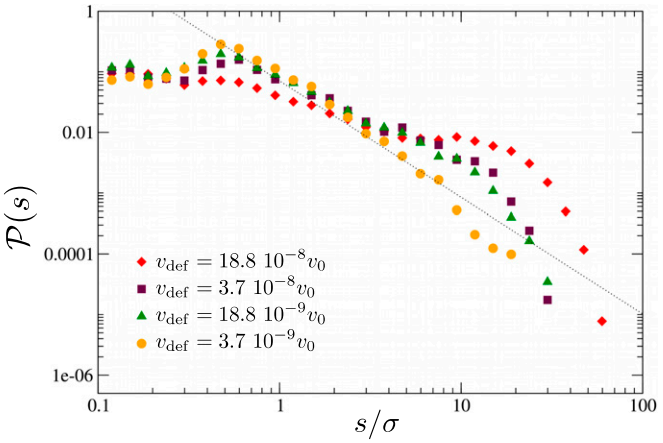

Fig. 4. Distribution of avalanche sizes displays scaling. Distribution of avalanche sizes s for different driving rates v_{def}. The scaling behavior is observed at low driving rates.

avalanches are triggered by much shorter scale events such as the nucleation of dislocation dipoles, tetramers, etc., dislocation reactions, and limited glide flow, rather than to the long range correlated glide of several dislocations. One could then anticipate that the size of these avalanches could not span so many orders of magnitude as in conventional geometries, where both the number as well as the displacements of topological defects are not so limited. A natural consequence of this observation is a larger exponent value characterizing the decay of the size distribution of these plastic events.

Indentation of a Spherical Shell of Repulsive Particles. To better understand the microscopic rearrangements occurring in a plastically deforming shell, we inspect a simple situation mimicking an indentation process. To this end, we approach quasistatically a linearly repulsive planar wall toward the particle shell. Particles remain essentially confined to the spherical template, but as stated in *Model*, deviations from the template are allowed for a cost. Furthermore, we do not take into account interactions between the repulsive wall and the spherical template, which is supposed to remain intact along the process. In this case, indentation leads to accumulation of stress until a crack opens up in the shell, near the indentation area, after achieving a threshold stress value (Fig. S4).

If we consider colloidal particles that interact through a pairwise repulsive potential of the form $V(r) \sim 1/r$, we favor plastic deformation, as opposed to the abrupt cracking near the indented zone that we observe in Lennard-Jones shells (Fig. S4). Such potential does not have a characteristic energy scale associated, and colloidal particles should not overcome a threshold energy value to start receding over the surface. We observe a smooth crossover from the initial elastic regime to a cavitation regime once the particles near the pushing wall have displaced themselves a distance of the order of the lattice spacing. The gradual opening of a hole on the spherical shell allows visualization of the rearrangement of the topological defect structure.

We consider N particles initially located at the interface of a perfect spherical drop in a scarred low-energy particle configuration (see the single snapshot illustrated in Fig. 5*A* for a crystal consisting of $N = 612$ particles). We model the short-range repulsion attributable to the planar wall with a potential of the form $V_r(d_w) = V_0 d_w^{-12}$, with d_w being the dimensionless separation of each particle from the repulsive wall. In this initial configuration, we can identify 12 positive disclinations in excess on the crystal, as expected. Fig. 5*A* shows six positively charged disclination strings or scars on the visible hemisphere. Five- and sevenfold sites are colored in red and green, respectively.

In general, the cavitation of the shell changes the topology of the crystal: according to the Euler theorem, the number of $q = +1$ excess disclinations needed to triangulate a surface is equal to $n = 6\chi$, where χ is the Euler characteristics, a topological invariant of the surface. In particular, $\chi = 2$ for a closed surface (e.g., a sphere) corresponding to $n = 12$ excess disclinations and $\chi = 1$ for an open surface (e.g., a sphere with a hole), so that $n = 6$ excess disclinations are needed. Hence, once the hole is created, the Euler theorem then implies that only 6 excess disclinations are necessary instead of the 12 originally present in the crystal. Our goal in this section is to investigate the dynamic reorganizations undergoing this process. Notice that the definition of disclination charge for particles at the edge of the crystal q_s has to be changed to $q_s \equiv 4 - c_s$, because 4 is the regular coordination number for a particle at the edge of a perfect triangular lattice. Hence, positive disclinations correspond to threefold coordinated particles at the lattice edge and negative disclinations to fivefold coordinated particles.

Having this in mind, we see that indeed fivefold coordinated particles located at the edge of the cavity, each contributing a disclination charge of $q_s = -1$, compensate the unnecessary excess disclination charge in the presence of a hole. To be precise, Fig. 5*B* shows four negatively charged disclinations and a negatively charged disclination scar, which compensate the unnecessary five positively charged scars still present in the visible hemisphere. Ideally, these five pairs of opposite-charged disclination structures should annihilate to reduce their energy cost, but disclinations themselves do no seem to be able to flow in the crystal. Instead, we observe a new physical mechanism that allows the pairs eventual annihilation. Disclination scars grow whenever new dislocations, which are nucleated in pairs of opposite Burgers vectors (dislocation dipoles such as the one in Fig. 5*B*), are able to attach to the existing disclination structures. For instance, the nucleation of new dislocations gives rise to the new −1 scar that emanates from a $q_s = -2$ negative disclination located at the edge of the void in Fig. 5*B*, the region under higher stress concentration where dislocation nucleation is thus more favorable. Moreover, the growth of this scar also represents the flow of the excess disclination charge, which can now be located at the other end of the growing scar.

The snapshot in Fig. 5*C* shows the appearance of two neutral grain boundaries ensuing this delocalization process, which allows the annihilation of two pairs of oppositely charge disclination structures. A neutral grain boundary does not have a

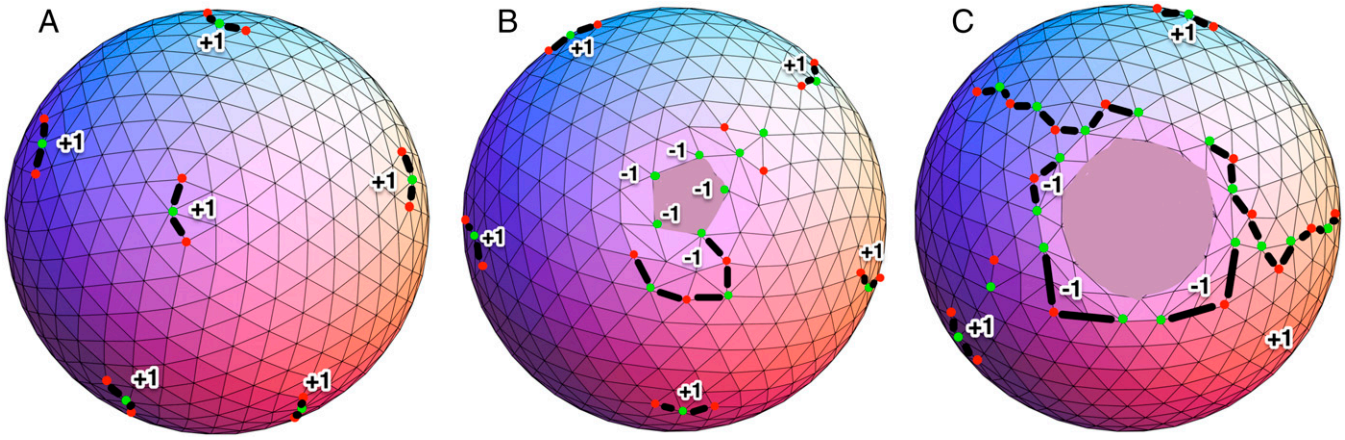

Fig. 5. The indentation of a spherical shell leads to the rearrangement of disclination structures. The evolution of the morphology of an indented crystalline spherical shell containing $N = 612$ particles as a function of time. As a repulsive flat tip approaches the interface, a hole opens up on the shell. (*A*) Before the cavitation of the curved crystalline structure, six disclination structures are present on the visible hemisphere. (*B*) After the cavitation of the shell, disclination charges of the opposite sign appear at the edge of the hole to fix the number of geometrically necessary defects under the new topological conditions. (*C*) The annihilation of pairs of opposite charged disclinations occurs progressively in time with the delocalization of these defects into neutral grain boundaries.

net disclination charge, and therefore, a grain boundary is a much less energy-costly topological defect, which could also be gradually annihilated through dislocation reactions at a later stage. The remaining three negatively charged disclinations near the void in Fig. 5*C* have also attached a new dislocation, and by doing so, they have moved from their previous position. In general, we observe that this process is indeed the microscopic mechanism by which disclinations and scars move and rearrange through the crystal: by multiple reactions with newly nucleated dislocations, which in turn only occurs if enough internal shear stress has been accumulated.

Discussion

In this paper, we have shown that the internal stress built up in a curved crystalline particle shell under load can give rise to fracture and plastic phenomena that, on the one hand, reflect the specificity of the chosen geometry, mainly because geometrically necessary rotational topological defects represent the key actors of irreversible deformation, but, on the other hand, exhibit features that are similar to those observed in flat geometries such as stress drops, crackling noise, and defect-induced crack nucleation.

In bulk plasticity, dislocation nucleation and motion generally serve to accommodate and release elastic shear stress accumulated in deformed crystals. The complexity of this process changes according to the scale of the crystal, to its microstructural features, and to the details of the deformation protocol. Once formed, dislocation dipoles usually unbind and dislocations glide parallel to their Burgers vector in opposite directions, giving rise to conspicuous stress drops in the stress–strain curves or plastic avalanches. For instance, in deformed flat colloidal crystals, one observes the motion of isolated dislocations reacting with grain boundaries (35). Likewise, in curved geometry, one expects that internal shear stress should be, at least partly, released with the migration of disclinations and dislocations over the crystalline interface. However, how is this motion taking place at the microscale?

The curvature of a sphere demands the presence of twelve fivefold disclinations in excess, usually in the form of grain-boundary scars, which have a net disclination charge. The enormous cost of disclinations and scars in a planar crystal in equilibrium conditions prevents their formation in flat geometries. Our results show that plastic deformation of curved crystals occurs through the rearrangement of these scars. In particular, we observe that scars rearrange intermittently through the assistance of new dislocations, which enable to modify their length and to reorient them through multiple reactions. Moreover, dislocations do not glide over long distances on curved crystal shells before such reactions occur. We thus observe plastic avalanches in curved shells undergoing irreversible deformation, but the size of these avalanches does not span as many orders of magnitude as in conventional geometries. We report a larger value for the exponent τ characterizing the power law decay of the size distribution of these plastic events, which indeed implies that large avalanches are more rare.

This work could stimulate further study of the out-of-equilibrium dynamics of topological defects in crystalline curved shells, and, as happens in bulk structures, it would be worthwhile investigating if crystalline shells share some characteristics with similar but amorphous assemblies of particles (36). Our results could be relevant to understand the mechanics of capsules made by active colloidal Janus particles (19), topologically constrained active structures (37), and other biostructured soft materials.

ACKNOWLEDGMENTS. C.N., A.L.S., and S.Z. are supported by European Research Council Advanced Grant 291002. S.Z. acknowledges support from Academy of Finland FiDiPro (Finland Distinguished Professor) Program Project 13282993. M.C.M. acknowledges financial support from the Ministerio de Economía y Competitividad (Spain) through Grants FIS2010-21781-C02-02, FIS2013-47282-C2-1-P, and MAT2015-69777-REDT.

1. Hirsch A (2010) The era of carbon allotropes. *Nat Mater* 9(11):868–871.
2. Ovidko I (2012) Review on grain boundaries in graphene. Curved poly- and nanocrystalline graphene structures as new carbon allotropes. *Rev Adv Mater Sci* 30(3):201–224.
3. Schneider S, Gompper G (2005) Shapes of crystalline domains on spherical fluid vesicles. *Europhys Lett* 70(1):136.
4. Dubois M, et al. (2001) Self-assembly of regular hollow icosahedra in salt-free catanionic solutions. *Nature* 411(6838):672–675.
5. Lipowsky P, Bowick MJ, Meinke JH, Nelson DR, Bausch AR (2005) Direct visualization of dislocation dynamics in grain-boundary scars. *Nat Mater* 4(5):407–411.
6. Lidmar J, Mirny L, Nelson DR (2003) Virus shapes and buckling transitions in spherical shells. *Phys Rev E Stat Nonlin Soft Matter Phys* 68(5 Pt 1):051910.
7. Zandi R, Reguera D, Bruinsma RF, Gelbart WM, Rudnick J (2004) Origin of icosahedral symmetry in viruses. *Proc Natl Acad Sci USA* 101(44):15556–15560.
8. Zandi R, Reguera D (2005) Mechanical properties of viral capsids. *Phys Rev E Stat Nonlin Soft Matter Phys* 72(2 Pt 1):021917.
9. Bausch AR, et al. (2003) Grain boundary scars and spherical crystallography. *Science* 299(5613):1716–1718.
10. Stratford K, Adhikari R, Pagonabarraga I, Desplat JC, Cates ME (2005) Colloidal jamming at interfaces: A route to fluid-bicontinuous gels. *Science* 309(5744):2198–2201.
11. Ramos L, Lubensky TC, Dan N, Nelson P, Weitz DA (1999) Surfactant-mediated two-dimensional crystallization of colloidal crystals. *Science* 286(5448):2325–2328.
12. Dinsmore AD, et al. (2002) Colloidosomes: Selectively permeable capsules composed of colloidal particles. *Science* 298(5595):1006–1009.
13. Dodgson MJW, Moore MA (1997) Vortices in a thin-film superconductor with a spherical geometry. *Phys Rev B* 55(6):3816–3831.
14. Pérez-Garrido A, Dodgson MJW, Moore MA (1997) Influence of dislocations in thomson's problem. *Phys Rev B* 56(7):3640–3643.
15. Bowick MJ, Nelson DR, Travesset A (2000) Interacting topological defects on frozen topographies. *Phys Rev B* 62(13):8738–8751.
16. Einert T, Lipowsky P, Schilling J, Bowick MJ, Bausch AR (2005) Grain boundary scars on spherical crystals. *Langmuir* 21(26):12076–12079.
17. Irvine WT, Bowick MJ, Chaikin PM (2012) Fractionalization of interstitials in curved colloidal crystals. *Nat Mater* 11(11):948–951.
18. Dommersnes P, et al. (2013) Active structuring of colloidal armour on liquid drops. *Nat Commun* 4(3066):2066.
19. Rozynek Z, Mikkelsen A, Dommersnes P, Fossum JO (2014) Electroformation of Janus and patchy capsules. *Nat Commun* 5(3945):3945.
20. Bowick M, Cacciuto A, Nelson DR, Travesset A (2002) Crystalline order on a sphere and the generalized Thomson problem. *Phys Rev Lett* 89(18):185502.
21. Bowick MJ, Cacciuto A, Nelson DR, Travesset A (2006) Crystalline particle packings on a sphere with long-range power-law potentials. *Phys Rev B* 73(2):024115.
22. Vitelli V, Lucks JB, Nelson DR (2006) Crystallography on curved surfaces. *Proc Natl Acad Sci USA* 103(33):12323–12328.
23. Bowick MJ, Giomi L (2009) Two-dimensional matter: Order, curvature and defects. *Adv Phys* 58(5):449–563.
24. Bowick M, Shin H, Travesset A (2007) Dynamics and instabilities of defects in two-dimensional crystals on curved backgrounds. *Phys Rev E Stat Nonlin Soft Matter Phys* 75(2 Pt 1):021404.
25. García NA, Register RA, Vega DA, Gómez LR (2013) Crystallization dynamics on curved surfaces. *Phys Rev E Stat Nonlin Soft Matter Phys* 88(1):012306.
26. Miguel MC, Vespignani A, Zapperi S, Weiss J, Grasso JR (2001) Intermittent dislocation flow in viscoplastic deformation. *Nature* 410(6829):667–671.
27. Zaiser M (2006) Scale invariance in plastic flow of crystalline solids. *Adv Phys* 55(1):185–245.
28. Plimpton S (1995) Fast parallel algorithms for short-range molecular dynamics. *J Comput Phys* 117(1):1–19.
29. Dimiduk DM, Woodward C, Lesar R, Uchic MD (2006) Scale-free intermittent flow in crystal plasticity. *Science* 312(5777):1188–1190.
30. Greer JR, Hosson JTD (2011) Plasticity in small-sized metallic systems: Intrinsic versus extrinsic size effect. *Prog Mater Sci* 56(6):654–724.
31. Smith EH (1994) *Mechanical Engineer's Reference Book* (Butterworth-Heinemann Ltd., Oxford, England), 12th Ed.
32. Sethna JP, Dahmen KA, Myers CR (2001) Crackling noise. *Nature* 410(6825):242–250.
33. Ispánovity PD, et al. (2014) Avalanches in 2D dislocation systems: Plastic yielding is not depinning. *Phys Rev Lett* 112(23):235501.
34. Moretti P, Cerruti B, Miguel MC (2011) Yielding and irreversible deformation below the microscale: Surface effects and non-mean-field plastic avalanches. *PLoS One* 6(6):e20418.
35. Irvine WTM, Hollingsworth AD, Grier DG, Chaikin PM (2013) Dislocation reactions, grain boundaries, and irreversibility in two-dimensional lattices using topological tweezers. *Proc Natl Acad Sci USA* 110(39):15544–15548.
36. Cui M, Emrick T, Russell TP (2013) Stabilizing liquid drops in nonequilibrium shapes by the interfacial jamming of nanoparticles. *Science* 342(6157):460–463.
37. Keber FC, et al. (2014) Topology and dynamics of active nematic vesicles. *Science* 345(6201):1135–1139.